



Vegetation pattern shift as a result of rising atmospheric CO₂ in arid ecosystems

Sonia Kefi^{a,*}, Max Rietkerk^a, Gabriel G. Katul^b

^a Department of Environmental Sciences, Copernicus Institute, Utrecht University, Heidelberglaan 2, PO Box 80115, 3508 TC Utrecht, The Netherlands

^b Nicholas School of the Environment and Earth Sciences, Box 90328, Duke University, Durham, NC 27708-0328, USA

ARTICLE INFO

Article history:

Received 19 January 2008

Available online 27 September 2008

Keywords:

Arid ecosystems
Spatial organization
Climate change
Increased CO₂
Desertification
Scale-dependent feedback

ABSTRACT

Arid ecosystems are expected to be among the ecosystems most sensitive to climate change. Here, we explore via model calculations how regular vegetation patterns, widely observed in arid ecosystems, respond to projected climatic shifts as provided by general circulation model output. In our model, the photosynthesis and respiration terms are explicitly linked to physiological attributes of the plants and are forced with the primary climatic drivers: atmospheric CO₂, air temperature, and precipitation. Under future climate scenarios, our simulations show that the system's fate depends on whether the enhancements to photosynthesis due to elevated atmospheric CO₂ outweigh the increases in respiration due to higher air temperatures and the increases in water stress due to lower rainfall. A scalar measure is proposed to quantify this balance between the changes in the three climate drivers. Our model results suggest that knowing how the three primary climate drivers are evolving may provide hints as to whether the ecosystem is approaching desertification.

© 2008 Elsevier Inc. All rights reserved.

1. Introduction

The projected increase in atmospheric greenhouse gases within the coming century will significantly impact global and regional temperatures with concomitant modifications of precipitation patterns (Houghton et al., 2001). Arid and semi-arid ecosystems, which cover about 40% of the Earth's terrestrial surface, are expected to be among the ecosystems most sensitive to such climatic changes (Agenda 21, 1993; Smith et al., 2000; Schröter et al., 2005; Thomas et al., 2005). According to the United Nation's Division for Sustainable Development, there are growing concerns that these climatic changes may lead to increased desertification, impacting approximately 25% of the world's population. Fingerprinting how arid ecosystems may respond to elevated atmospheric CO₂, and to the associated increases in air temperature and reduction in precipitation, remains a vexing research problem well beyond the scope of a single study. Here, we focus on the spatial organization of vegetation as a starting point to explore this problem.

Spatially regular vegetation patterns are well known in arid regions, where dense patches of vegetation alternate with bare soil (Barbier et al., 2006; Rietkerk and van de Koppel, 2008). Vegetation patches can consist of grasses and/or shrubs and/or trees, and occur on soils ranging from silty to clayey (Tongway and Ludwig,

2001). Different shapes of patches have been observed, such as stripe ('tiger bush'), gap, labyrinth or spot patterns ('leopard bush'). These regular patterns have been described throughout the world (Valentin et al., 1999). The spatial scale of vegetation patches is in the order of tens or hundreds of meters, depending on topographic gradients and rainfall (Lejeune et al., 1999; Barbier et al., 2006).

Over the past decade, much progress has been made in linking observed spatial organization of the vegetation in arid ecosystems with positive feedback between plants and limiting resources (mainly water) (Rietkerk et al., 2004). The origin and maintenance of these spatial patterns received considerable attention, and several feedback mechanisms have been explored, all successful at reproducing these patterns. Lefever and Lejeune (1997), Lejeune et al. (1999) and Lejeune and Tlidi (2002) developed a phenomenological model, where pattern formation relies on plant characteristics only. In their model, pattern formation is due to short-range facilitation of plants under their aerial structures, together with long-range competition between plants by overlapping root zones. The ratio crown/root area determines the scale of the patterns. Klausmeier (1999) proposed a model that explicitly considers soil water dynamics: plants increase local water availability in the soil, which favors their growth (see Ursino (2005) and Ursino and Contarini (2006) for recent extensions of this model). von Hardenberg et al. (2001) and Meron et al. (2004) suggested a model, also incorporating soil water dynamics, where two main processes are responsible for the positive feedback. Higher biomass reduces evaporation and increases infiltration, leading to higher soil moisture availability and thus to higher biomass. Also, higher biomass increases the extent of

* Corresponding author.

E-mail addresses: kefi@geo.uu.nl (S. Kefi), rietkerk@geo.uu.nl (M. Rietkerk), gaby@duke.edu (G.G. Katul).

the rooting zone, leading to higher soil water availability and thus to higher biomass (so-called root-augmentation feedback). Okayasu and Aizawa (2001) and Rietkerk et al. (2002) (hereafter referred to as R2002) introduced models in which the water budget is decomposed into a subsurface and a simplified surface component, permitting these two reservoirs to interact differently with vegetation. In these two models, surface water infiltrates faster into vegetated ground than into bare soil, leading to a net displacement of surface water to vegetation patches, which increases vegetation growth. This leads to a positive feedback locally. At the same time, resource concentration underneath the vegetation causes resource depletion farther away, and thus a negative feedback. This results in a scale-dependent feedback, consisting of a short-range positive feedback and a long-range negative feedback. Saco et al. (2007) coupled R2002 to a landform evolution model to account for erosion–deposition mechanisms and their effect on vegetation patterns and micro-topography. Similarly to Okayasu and Aizawa (2001), Rietkerk et al. (2002) and Saco et al. (2007), Gilad et al. (2004, 2007a) studied a three-variable model that distinguishes between soil water and surface water, but their model includes root-augmentation feedback additional to infiltration feedback.

Despite differences between the models in the precise description of feedback between vegetation and water availability, they all share several mathematical features: (1) their canonical structure resembles an activation–inhibition system (Cross and Hohenberg, 1993), (2) when rainfall decreases, a certain sequence of vegetation patterns emerges, namely a transformation from uniform cover to gaps, to labyrinths, to spots and ultimately to uniform bare soil, and (3) transition from a vegetated system to a desert can happen in a discontinuous way – often labeled as a “catastrophic shift”. From this, the hypothesis follows that certain patterns, now observable from satellite remote sensing products (e.g. IKONOS or QUICKBIRD), could be used as indicators of proximity to desertification thresholds (Rietkerk et al., 2004).

Currently, rainfall and evaporation rates are the only climatic parameters taken into account in all these models. However, climate change also relates to persistent increases in the concentration of atmospheric CO₂ ([CO₂]) and air temperature. Increases in [CO₂] are known to increase photosynthesis, biomass and water-use efficiency in many plant species (e.g. Larcher (2003), Smith et al. (2000), Oren et al. (2001), Shaw et al. (2002), Gill et al. (2002) and Körner et al. (2005)). Conceptual models suggest that arid and semi-arid ecosystems, where primary productivity is strongly limited by water, may be highly responsive to increased [CO₂], because the increased plant water-use efficiency can alleviate water stress and contribute to increases in primary production (e.g. Melillo et al. (1993)). The interplay between changes in rainfall, air temperature and [CO₂] determine how the coupled carbon–water cycles will be altered, and subsequently, how the scale-dependent feedback and its signature in the vegetation patterns will respond. In a recent analysis of remotely sensed data from southern Niger, Barbier et al. (2006) showed that the decrease in rainfall over recent decades (1956–1996) has been accompanied by a detectable shift from homogeneous vegetation cover to gap patterns. This finding is promising because of the sequence of pattern shapes along gradients predicted by the models (from homogeneous vegetation cover to gaps, labyrinths, spots and bare soil). Looking at the shape of the vegetation patterns can therefore provide clues as to how far the system is from desertification thresholds (i.e. from a desert). When rising temperature and [CO₂] are incorporated into existing mathematical models of pattern formation, how do the three interacting climatic drivers (CO₂, air temperature and precipitation) affect the vegetation patterns? Is the range of predicted climate change over the next century sufficient to induce shifts in vegetation patterns of arid ecosystems?

To address these questions, we focus on the approach of R2002 because the main driver for pattern formation does not require particular root distribution/uptake functions, often difficult to determine a priori. The R2002 model retains the essential spatial patterns in soil moisture and surface water, thereby providing a direct pathway to couple the hydrologic (surface and sub-surface) and the carbon cycles. The main novelties of the proposed study are (1) to relate the photosynthesis and respiration terms in R2002 explicitly to physiological attributes that can interact with the three climatic drivers: CO₂, air temperature, and precipitation, and (2) to explore the effect of projected climatic shifts, as provided by general circulation models (GCMs), on vegetation patterns.

2. The model

For completeness, we provide a review of the basic formulation of the R2002 model, followed by a description of how the hydrologic and carbon budgets are revised to account for the three external climatic drivers: precipitation, temperature, and [CO₂]. In R2002, three state variables are considered: plant density P (g m⁻²), soil water W (mm) and surface water O (mm). R2002 assumes that rainfall events in arid and semi-arid ecosystems occur at an intensity exceeding the infiltration capacity of the soil. Hence, part of the rainwater infiltrates into the soil, while the remainder produces surface water and runoff routed to other spatial locations. The infiltration rate is assumed to asymptotically approach a maximum with increasing plant density, an assumption supported by field observations reported in Rietkerk et al. (2000). There are two plausible reasons why the infiltration rate increases with increasing biomass: (1) the presence of vegetation reduces the surface crust often characterized by low hydraulic conductivity values, and (2) the rooting system increases the fraction of macropore sites near the soil surface (Katul et al., 1997). Lateral flow of surface water is driven by static pressure differences and can be described with a single diffusion term. In the absence of terrain variations, the dynamics of surface water depth are modeled as:

$$\frac{\partial O}{\partial t} = R - \alpha O \frac{P + k_2 W_o}{P + k_2} + D_o \Delta O, \quad (1)$$

with R the rainfall (mm d⁻¹), α the maximum infiltration rate (d⁻¹), k_2 the saturation constant of water infiltration (g m⁻²), W_o a measure of the infiltration contrast between vegetated and bare soil (dimensionless), Δ is the Laplace operator in x and y , and D_o the diffusion coefficient of surface water (m² d⁻¹).

The infiltrated soil water is lost due to plant uptake, to evaporation and drainage, and to lateral subsurface flow because of capillary forces. Soil water dynamics are modeled as follows:

$$\frac{\partial W}{\partial t} = \alpha O \frac{P + k_2 W_o}{P + k_2} - T_r - r_w W + D_w \Delta W, \quad (2)$$

with r_w the specific soil water loss due to evaporation and drainage (d⁻¹) and D_w the diffusion coefficient of soil water (m² d⁻¹).

From now on, we start presenting new development of the model compared with R2002. Water uptake by plants is described by a transpiration term T_r , whose driving force is the difference between saturated and actual specific humidity:

$$T_r \approx g_{\text{canopy}} (q^* - q_a), \quad (3)$$

where g_{canopy} is the bulk canopy conductance to H₂O transport (mm d⁻¹), and q (dimensionless) is the specific humidity.

Here, g_{canopy} is assumed to be a saturation function of soil water availability and can be expressed as:

$$\begin{aligned} g_{\text{canopy}} &= g_{\text{H}_2\text{O}} \frac{W}{W + k_1} L_{\text{AI}} = g_{\text{H}_2\text{O}} \frac{W}{W + k_1} \alpha_2 P \\ &= \gamma g_{\text{CO}_2} \frac{W}{W + k_1} \alpha_2 P, \end{aligned} \quad (4)$$

where g_{H_2O} is now interpreted as a maximum leaf conductance to H_2O ($mm\ d^{-1}$) (i.e. stomatal conductance when all the stomatal pores are open to full capacity), k_1 is the half-saturation constant of specific growth and water uptake ($mm\ d^{-1}$), L_{AI} is the leaf area index (dimensionless, $L_{AI} \approx \alpha_2 P$), α_2 is the conversion coefficient of biomass into L_{AI} ($m^2\ g^{-1}$), and g_{CO_2} is the maximum leaf conductance to CO_2 ($mol\ m^{-2}\ d^{-1}$) related to g_{H_2O} by a conversion coefficient γ accounting for the difference in molecular diffusivities of CO_2 and H_2O .

In Eq. (3), the specific humidity is defined as $q = \rho_v / \rho_d$ with ρ_v and ρ_d the densities of water vapor and dry air, respectively ($kg\ m^{-3}$). The relationship between q and vapor pressure can be derived from Dalton's law as follows:

$$\rho_d = \frac{p - e}{R_d T_a}, \quad (5)$$

$$\rho_v = \frac{0.622e}{R_d T_a}, \quad (6)$$

where p is the total atmospheric pressure (Pa), e is the partial pressure of the water vapor (Pa), R_d is gas constant for dry air ($J\ kg^{-1}\ K^{-1}$), T_a is absolute temperature (K), $0.622 = 18/29$ is the ratio of molecular weights of water and dry air.

Noting that $p \gg e$ results in $q \approx 0.622 e/p$, $q^* = 0.622 e^*/p$, and

$$T_r = \gamma g_{CO_2} \alpha_2 \frac{W}{W + k_1} P \frac{0.622}{p} e^* \left(1 - \frac{e}{e^*}\right). \quad (7)$$

The saturation vapor pressure (in kPa) can be determined from mean air temperature T (in °C) using the standard Clausius–Clapeyron equation,

$$e^*(T) = 0.611 \exp\left(\frac{17.502 T}{T + 240.97}\right). \quad (8)$$

In a first order analysis, we assume that the atmospheric pressure (in kPa) is hydrostatic, thereby varying only with site elevation (EL , m; in this study $EL = 0$), and is given by

$$p = 101.3 \exp\left[\frac{-EL}{8200}\right]. \quad (9)$$

Noting that air relative humidity (Rh) is defined as e/e^* explicitly yields

$$T_r = \gamma g_{CO_2} \alpha_2 \frac{0.622}{p} e^*(T)(1 - Rh) \frac{W}{W + k_1} P. \quad (10)$$

Hence, T_r is now unambiguously linked to the physiological attributes of stomata through g_{CO_2} , and to the external drivers Rh and T .

Plant growth is modeled as an imbalance between carbon gain through photosynthesis (which depends on $[CO_2]$) and carbon loss by respiration (modeled as a function of temperature and respiring biomass). Here, we assume that the total respiration term is primarily controlled by autotrophic respiration, a reasonable first-order approximation in arid and semi-arid ecosystems (Williams and Albertson, 2005). Research on seed dispersal indicates that the seed bank is mainly concentrated in the vegetation patches (van Rheede van Oudtshoorn and van Rooyen, 1999; Mauchamp et al., 2001; Montaña et al., 2001). It has been shown that 90% of the seeds of *F. Cernua*, the dominant vegetation cover of bands in Mexico, are beneath the adult crown, while 10% of the seeds are dispersed by runoff water, wind, domestic and wild animals (Montaña et al., 2001). This order of magnitude is confirmed by other studies (Montaña et al., 1990). Plant dispersal, through seeds or vegetated reproduction, may therefore be approximated by a

diffusion term. With these approximations, the dynamics of plant biomass are modeled as

$$\frac{\partial P}{\partial t} = C_{\text{gain}} - R_{\text{esp}} P + D_p \Delta P. \quad (11)$$

The global variable P encompasses all the vegetation biomass present (above and below ground). The autotrophic respiration (second term) is well approximated by a Michaelis Q_{10} function (Larcher, 2003), given by

$$R_{\text{esp}} = R_b Q_{10}^{(T-10)/10}, \quad (12)$$

where R_b is a base respiration per unit of biomass (d^{-1}).

The carbon gain (first term) is proportional to the canopy photosynthesis,

$$C_{\text{gain}} = C_1 A_{n_{\text{canopy}}}, \quad (13)$$

where C_1 is the conversion coefficient of photosynthesis into biomass ($g\ mol^{-1}$), and $A_{n_{\text{canopy}}}$ the canopy photosynthesis ($mol\ m^{-2}\ d^{-1}$). $A_{n_{\text{canopy}}}$ is related to leaf physiological attributes by

$$A_{n_{\text{canopy}}} = L_{AI} A_{n_{\text{leaf}}} = L_{AI} g_{\text{leafCO}_2} C_a \left(1 - \frac{C_i}{C_a}\right), \quad (14)$$

with $L_{AI} = \alpha_2 P$ (i.e. foliage area per unit ground area is proportional to the standing biomass), $A_{n_{\text{leaf}}}$ is the leaf-level photosynthesis ($mol\ m^{-2}\ d^{-1}$), g_{leafCO_2} is as before, the leaf conductance to CO_2 ($mol\ m^{-2}\ d^{-1}$), and C_a the ambient CO_2 concentration ($mol\ mol^{-1}$), and C_i the effective canopy intercellular CO_2 concentration ($mol\ mol^{-1}$). Hence,

$$C_{\text{gain}} = C_a \left(1 - \frac{C_i}{C_a}\right) \alpha_2 C_1 g_{CO_2} \frac{W}{W + k_1} P. \quad (15)$$

With these approximations, the model can be formulated as:

$$\frac{\partial P}{\partial t} = c \alpha_2 g_{CO_2} \frac{W}{W + k_1} P - R_{\text{esp}} P + D_p \Delta P \quad (16)$$

with $c = C_a \left(1 - \frac{C_i}{C_a}\right) C_1$ and $R_{\text{esp}} = R_b Q_{10}^{\frac{T-10}{10}}$

$$\frac{\partial W}{\partial t} = \alpha O \frac{P + k_2 W_o}{P + k_2} - \alpha_2 \gamma g_{CO_2} \frac{W}{W + k_1} q P - r_w W + D_w \Delta W \quad (17)$$

with $q = q^* - q_a = \frac{0.622}{p} e^* (1 - Rh)$

$$\frac{\partial O}{\partial t} = R - \alpha O \frac{P + k_2 W_o}{P + k_2} + D_o \Delta O. \quad (18)$$

Table 1 summarizes the model parameters. Their values, taken from the literature, are given in the legends of the figures and in Appendix A.

2.1. Model assumptions and physiological attributes

Given the time scale of pattern formation (years to decades), we do not intend to precisely model short-term physiological processes on an event-by-event basis (e.g. immediately after rainfall). Rather, the model seeks to account for the primary effects of long-term climatic shifts on pattern formation. Rather than listing the numerous processes that we do not explicitly include here, we highlight several generic ones:

(1) *Root-augmentation feedback*. Besides the infiltration feedback, Gilad et al. (2004, 2007a) introduced a root-augmentation feedback in their model. As plants grow, their root system becomes larger. A larger root system allows the plants to probe larger soil

Table 1
Table of parameters

Class	Symbol	Interpretation	Unit
Parameter	k_1	Half-saturation constant of specific plant growth and water uptake	mm d ⁻¹
	k_2	Saturation constant of water infiltration	g m ⁻²
	α	Maximum infiltration rate	d ⁻¹
	W_0	Measure of the infiltration contrast between vegetated and bare soil	–
	r_w	Specific soil water loss due to evaporation and drainage	d ⁻¹
	D_p	Plant dispersal	m ² d ⁻¹
	D_w	Diffusion coefficient for soil water	m ² d ⁻¹
	D_0	Diffusion coefficient for surface water	m ² d ⁻¹
	C_1	Coefficient of conversion of photosynthesis (mol) into biomass (g)	g mol ⁻¹
	g_{CO_2}	Maximal leaf conductance to CO ₂	mol m ⁻² d ⁻¹
	γ	Conversion coefficient from maximal leaf conductance to water vapour (mm d ⁻¹) to maximal leaf conductance to CO ₂ (mol m ⁻² d ⁻¹)	mm m ² mol ⁻¹
	α_2	Conversion coefficient of biomass into L_{AI}	g ⁻¹ m ²
	C_a	Ambient CO ₂ concentration	mol mol ⁻¹
	C_i	Intercellular CO ₂ concentration (in the leaf)	mol mol ⁻¹
	R_b	Respiration per unit of biomass	d ⁻¹
	Q_{10}		Dimensionless
	T	Temperature	°C
	p	Total pressure in the air	kPa
	$e(T)$	Vapor pressure at T	kPa
	$e^*(T)$	Saturated vapor pressure	kPa
	Rh	Relative humidity, $e(T)/e^*(T)$	Dimensionless
	R	Rainfall	mm d ⁻¹
	W_{UE}	Water use efficiency $W_{UE} = \gamma_c \frac{C_a(1 - \frac{C_i}{C_a})}{e^*(T)(1 - Rh)}$	mol _{CO₂} mol _{H₂O} ⁻¹
γ_c	Unit conversion factor for water use efficiency	kPa	
Φ	Measure for the carbon input to the system $\Phi = WUE \times R$ $\Phi^{(i)}$ is for climate scenario i , $i = 1, 2, 3$	mol _{CO₂} mol _{H₂O} ⁻¹ mm d ⁻¹	
σ	Measure of how the changes in C_a , T and R balance each other in future climatic scenarios as compared to current climate. $\sigma^{(i)}$ is for climate scenario i , $i = 1, 2, 3$. $\sigma^{(i)} = \frac{\Phi^{(i)}}{\Phi^{(0)}}$	Dimensionless	
Variable	P	Plant density	g m ⁻²
	W	Soil water	mm
	O	Surface water	mm

volumes and thus potentially increases the amount of resource that a plant at a given point in space can access. This feedback does not affect the general sequence of biomass patterns, but it does affect the soil–water distribution, and therefore can have implications on questions such as ecosystem engineering and species coexistence (questions which are not addressed in this paper). In this paper, we decided to study the role of the infiltration feedback in isolation, which has been proved and measured in the field (e.g. Rietkerk et al. (2000)).

(2) *Erosion-biomass feedback.* Saco et al. (2007) coupled R2002 to a landform evolution model to account for sediment redistribution in runoff surface water. They studied the effect on vegetation patterns and on micro-topography. The model reproduced vegetation patterns, as obtained by other models of arid ecosystem dynamics, and a stepped micro-topography, as observed in the field. Here, we focused on the vegetation patterns and we did not address the erosion–deposition mechanisms.

(3) *Feedback processes from vegetation to local climate.* Vegetation patterns occur at spatial length scales varying between a few tens of meters and a few hundred meters (Lejeune et al., 1999), and hence we assume here that their impact on atmospheric boundary layer processes is likely to be minimal, at least on the decadal time scales of interest. Dekker et al. (2007) studied how local precipitation could be affected by evapotranspiration rates that, in turn, depend on the vegetation patterns.

(4) *Nutrient cycling (Nitrogen and Phosphorus) and their effects on photosynthesis, respiration, and carbon allocation.* Our model assumes that water is a much more limiting resource than Nitrogen (and Phosphorus) availability. Hence, we neglect nutrient cycling and the soil nitrogen budget. It would be possible to account for a simplified Nitrogen balance budget, by making α_2 vary with available Nitrogen (see Porporato et al. (2003)). However, given the

uncertainties in future Nitrogen deposition and the vast number of parameters needed in the Nitrogen budget, we assume that α_2 remains constant.

(5) *Effects of elevated [CO₂] on physiological parameters.* (e.g. α_2 , g_{CO_2} , Q_{10} , C_i/C_a , and R_b). Important to global change models is whether elevated [CO₂] alters leaf stomatal characteristics (e.g. Woodward (1987) and Gedney et al. (2006)). A synthesis study by Reid et al. (2003) examined the phenotypic response of stomatal index (SI), stomatal density (SD), and stomatal aperture (AP) to rising [CO₂] in 15 species after four years exposure to a field [CO₂] gradient ranging from 200 to 550 ppm. They concluded that there was no clear evidence that SI, SD, and AP significantly changed with increasing [CO₂], suggesting that g_{CO_2} , the maximal leaf conductance in the revision to R2002, does not need to be altered with elevated [CO₂]. This assumption is further supported by FACE experiments in a pine plantation and a hardwood forest, which suggest that the maximum bulk canopy conductance was minimally affected by elevated [CO₂] in South Eastern United States (Schäfer et al., 2002; Wullschlegel et al., 2002).

We do not have detailed measurements on how C_i/C_a , Q_{10} , and R_b change with elevated [CO₂] in arid ecosystems. However, we note that preliminary FACE experiments in a pine plantation (Katul et al., 2000) suggest that C_i/C_a remains approximately constant with elevated [CO₂]. Katul et al. (2000) demonstrated that when stomatal conductance was specified, the model with constant C_i/C_a performed no worse than the Farquhar model in reproducing leaf-level assimilation over a three year period for ambient and elevated CO₂ foliage. Moreover, these experiments suggest that Q_{10} increases under elevated [CO₂] for non-water stressed conditions. At the same stand, droughts tend to decouple respiration responses to temperature, and hence there is no clear consensus how Q_{10} would be altered under elevated [CO₂] in dry conditions. Given

the uncertainty in how Q_{10} and R_b change with elevated $[\text{CO}_2]$, we employ the simplest assumption and assume that they are independent from $[\text{CO}_2]$. In short, we will assume that increasing $[\text{CO}_2]$ will not significantly alter α_2 , g_{CO_2} , C_i/C_a , Q_{10} and R_b from their present state.

(6) *Rainfall dynamics*. It is well-known that specific rainfall patterns may cause major establishment and mortality events that change the state of arid ecosystems. The strong variability and unpredictability of rainfall is an integral part of arid ecosystems. However, in this study we only consider long-term average rainfall. We justify this choice because we are interested in the long-term integration of biomass occurring at a different temporal scale than the short-term rainfall dynamics. This approximation can be better justified for species such as woody species whose growth occurs at a larger timescale than rainfall variability (Gilad et al., 2007a). Recently, Guttal and Jayaprakash (2007) addressed the role of rainfall seasonality on vegetation dynamics in a model of semi-arid ecosystems. They show that seasonality of rainfall affects the system's dynamics in several ways, but the same sequence of patterns occurs along transition toward desertification than when rainfall seasonality is not included (the sequence is however shifted toward higher rainfall values). Ursino (2005) expanded the model of Klausmeier (1999) and investigated the effect of seasonal rainfall and intense showers on soils with limited storage capacity (Ursino and Contarini, 2006). D'Odorico et al. (2006) studied how random interannual climate fluctuations may determine the emergence of vegetation patterns.

(7) *Vegetation*. The model does not distinguish species or functional types. Vegetation is simply summarized in a unique variable, the plant biomass per unit ground area, which can be a mixture of life forms (grasses, shrubs, trees ...). Considering a global variable including all vegetal species present is justified for patterns formed by a one-species and in all cases where genotypic differences and age classes can be neglected. When several species are present, it amounts to assuming that the dominant species imposes its dynamics (Lejeune et al., 1999). Gilad et al. (2007b) recently proposed a model of arid ecosystem including two types of species, shrubs and grasses (see also Van Wijk and Rodriguez-Iturbe (2002)).

(8) *Vegetation adaptation to climate change*. As pointed by Jump and Peñuelas (2005), the predicted rate of climate change might overwhelm the adaptation rate in many native plant populations within arid ecosystems. Furthermore, given that our objective is to seek the maximum potential response of vegetation patterns to climate change, neglecting any adjustments of plant physiological characteristics due to adaptation provides a logical upper-limit.

Some of these assumptions have immediate consequences on the leaf (or canopy) water use efficiency (W_{UE}), which is defined as the ratio of photosynthesis to transpiration. In our model, W_{UE} is given by

$$W_{UE} = \gamma_c \frac{C_a(1 - \frac{C_i}{C_a})}{e^*(T)(1 - Rh)}, \quad (19)$$

where γ_c is a unit conversion factor. For a constant C_i/C_a (no adaptation), W_{UE} becomes independent of leaf (or canopy) conductance and only varies with climatic drivers. Hence, if $[\text{CO}_2]$ increases, but T (and Rh) is not altered from its present climatic state (as it is the case in FACE experiments), W_{UE} will increase in proportion to C_a . However, if both $[\text{CO}_2]$ and T increase, W_{UE} does not need to necessarily increase, given the exponential dependence of e^* on T in the Clausius–Clapeyron equation. Hence, the interplay between changes in T and $[\text{CO}_2]$ will have important consequences on the coupled carbon-water cycles, the positive feedback and pattern formation, if C_i/C_a is kept constant (i.e. no adaptation or down-regulation by the plant; see also Katul et al. (2003)).

To sum up, our final model is essentially R2002 with changes in prefactors. Our revised three-equation model cannot capture all the richness in ecosystem processes governing the cycling of carbon and water. In particular, the modeling of lateral movement as diffusion terms is a rough approximation, which can be quite unrealistic. Nevertheless, the inclusion of more realistic movement terms does not fundamentally alter the results (Gilad et al., 2004; Pueyo et al., 2008), and even such a simple model may be capable of discerning broad patterns in terms of ecosystem responses to changes in climatic forcing and possibly provide 'measurable' indicators as to the onset of desertification.

3. Analysis

We first explored spatially homogeneous solutions of the model. The parameter space that may induce regular patterns and the onset of regular patterns in future climatic scenarios are then derived analytically from linear stability analysis (in space and time). Spatially explicit simulations are conducted afterwards to diagnose whether other patterns form (due to nonlinearities in the model), as well as to compare the shape of the patterns in current and future climatic conditions.

3.1. The non-spatial model

Equilibrium points of the non-spatial model can be analytically calculated by setting the three equations (Eqs. (16)–(18)) simultaneously equal to zero ($\frac{dP}{dt} = 0$, $\frac{dW}{dt} = 0$, $\frac{dO}{dt} = 0$). For steady and uniform conditions, the model has two types of equilibria: an equilibrium consisting of no vegetation (or desert) ($P^* = 0$, $W^* = \frac{R}{r_w}$, $O^* = \frac{R}{\alpha W_o}$), and an equilibrium corresponding to a strictly positive vegetation density (also called non-trivial equilibrium) ($P^* = \frac{c g_{\text{CO}_2}}{q g_{\text{H}_2\text{O}}} (\frac{R}{R_{\text{resp}}} - \frac{r_w k_1}{c \alpha_2 g_{\text{CO}_2} - R_{\text{resp}}})$, $W^* = \frac{R_{\text{resp}} k_1}{c \alpha_2 g_{\text{CO}_2} - R_{\text{resp}}}$, $O^* = \frac{R}{\alpha} (\frac{P^* + k_2}{P^* + k_2 W_o})$) that exists when $R > \frac{r_w k_1 R_{\text{resp}}}{c \alpha_2 g_{\text{CO}_2} - R_{\text{resp}}}$ and $c \alpha_2 g_{\text{CO}_2} > R_{\text{resp}}$.

The non-trivial equilibrium is locally stable to spatially homogeneous perturbations when it exists.

3.2. Linear stability analysis

Linear stability analysis is used to determine whether regular patterns can form. The principle of this analysis is to investigate the fate of a small initial heterogeneity in an otherwise uniform system (Turing, 1952; Murray, 2002).

In more intuitive terms, the principle of the analysis is as follows. We start from a spatially homogeneous steady state of plant density, soil water and surface water (i.e. from the non-trivial equilibrium of the non-spatial model) in the conditions where this equilibrium is stable with respect to spatially homogeneous perturbations. Then, the linear stability analysis consists in adding or removing a small but spatially heterogeneous amount of plants, soil water and surface water. If these perturbations spatially grow, the system will develop to a new, spatially patterned steady state.

We call the patterns predicted by this method *Turing patterns* and the range of parameter values in which they occur *Turing instability range*. The Turing instability range can be analytically calculated, and the details of the analytical derivation are presented in Appendix B. We investigate the formation of Turing patterns for the 'exogenous' climatic parameters, and for the 'endogenous' soil–plant physiological parameters.

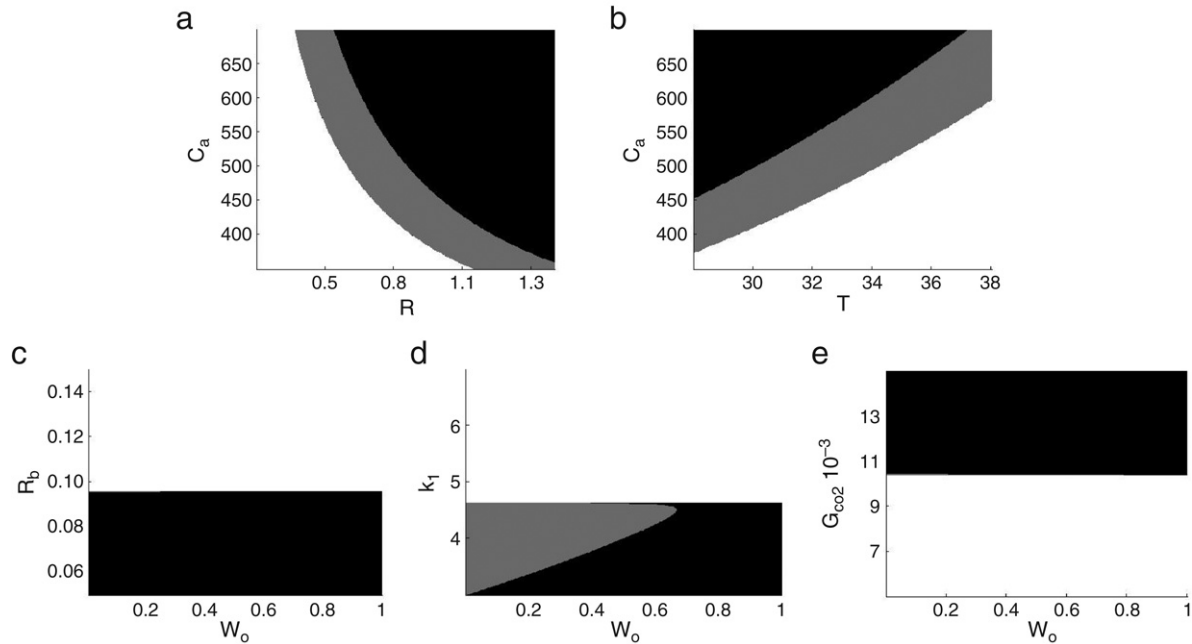


Fig. 1. Effect of climatic (first row) and soil/vegetation (second row) characteristics on the Turing instability range. Black: homogeneous vegetation, grey: Turing instability range, white: desert. Along the axes, R varies between 0.2 and 1.5 mm d^{-1} , T varies between 28 and 38 $^{\circ}\text{C}$, C_a varies between 350 and 700 ppm, W_o varies between 0.01 and 1, R_f varies between 0.05 and 0.15 d^{-1} , k_l varies between 3 and 7 mm, and g_{CO_2} varies between 5×10^3 and $15 \times 10^3 \text{ mol m}^{-2} \text{ d}^{-1}$. On graphs c and e, the Turing instability range is present but very small, between the homogeneous vegetation (black) and the desert (white) area. Other parameter values: $T = 28 ^{\circ}\text{C}$, $R = 1 \text{ mm d}^{-1}$, $C_a = 360 \text{ ppm}$. See Table 1 for the interpretation of the parameters and Appendix A for the value of the parameters not mentioned here.

3.3. Spatially explicit simulations

Two-dimensional numerical simulations were also performed. They correspond to Euler integration of the finite-difference equations resulting from the discretization of the diffusion operator. The spatial mesh consists of a grid of 500×500 cells for Figs. 1–3. For these figures, a ‘no flux of matter boundary condition’ at the border cells is assumed. The use of ‘periodic boundary conditions’ instead is not intuitively appealing because some parameter values change along the two directions. For Fig. 4, the spatial mesh consists of a grid of 200×200 cells with periodic boundary conditions. In case of periodic boundary conditions, any biomass that crosses a boundary of the simulated grid (e.g. last column) is reinserted at the opposite side (e.g. first column). It is as if the primary simulated grid were periodically replicated throughout space to form an infinite lattice.

For the current climate (Figs. 2, 3a–c, 4a–c), simulations were started by randomly introducing mature plants in 1% of the cells (for each of those cells: $P = 50 \text{ g m}^{-2}$, W and O : homogeneous equilibrium). For future climatic scenarios (Figs. 3d–l, 4d–l), the outcome of the model for current climate was used as an initial condition. Simulations were run until stationary patterns were reached (i.e. steady-state). The spatial domain is such that one cell is about 2×2 square meters, and the integration time step is daily.

3.4. Climatic scenarios

Three future climatic scenarios that bound the range of values predicted by the Hadley Center (see Cox et al. (2000)) were selected. These climatic predictions use a coupled atmosphere–ocean general circulation model (HadCM3) and assume that future greenhouse gas emissions follow the so-called IS92a scenario, in which the atmospheric concentration of carbon dioxide doubles over the course of the 21st century ($[\text{CO}_2]$ from 350 to 700 ppm). This is referred to as the ‘business as usual’ scenario, which assumes mid-range economic growth but no measures to reduce greenhouse-gas

Table 2

Climatic scenarios

	$[\text{CO}_2]$ (ppm)	T ($^{\circ}\text{C}$)	R (mm d^{-1})
Scenario 1	+340	+5	–0.2
Scenario 2	+340	+7.5	–0.35
Scenario 3	+340	+10	–0.5

Difference compared to current climate ($[\text{CO}_2] = 360 \text{ ppm}$, $T = 28 ^{\circ}\text{C}$ and $R = 1 \text{ mm d}^{-1}$).

emissions. The model predicts the differences between the current climate, conventionally defined as 1960–1990, and the climate of the end of the 21st century, taken to be 2070–2100.

For the Sahel, the Hadley Center projects long-term changes in annual temperature to range from +3 to +10 $^{\circ}\text{C}$, and annual precipitation to range from –0.2 to –0.5 mm d^{-1} . With these ranges, we summarize the climatic scenarios in Table 2.

For the Sahel area, we used yearly average data for rainfall and temperature from Dakar (Senegal), Nouakchott (Mauritania), Bamako (Mali), Ouagadougou (Burkina Faso), Niamey (Niger) and Khartoum (Sudan) to estimate current climatic conditions. Averaging these data results in a current climate with annual temperature and rainfall $T = 28 ^{\circ}\text{C}$, $R = 1 \text{ mm d}^{-1}$, respectively, and mean relative humidity $Rh = 0.4$. Current $[\text{CO}_2]$ is taken as the global mean of 360 ppm.

Based on several global climatic models (GCM), atmospheric relative humidity appears invariant to changes in greenhouse warming (e.g. see Kumagai et al. (2004) for various references), and we also assumed that Rh is unaltered in future climatic scenarios.

4. Results

The results section first describes the existence of stable Turing patterns for the plausible range of climatic (exogenous) conditions and parameter (endogenous) space. The explicit form of these patterns is presented next, using numerical simulations. We then track how various climatic scenarios induce pattern shifts, starting

Fig. 2. Effect of climatic parameters on explicit vegetation and soil water patterns. First row: vegetation density. Second row: soil water. A white color indicates zero density. Darker colors (from gray to black) indicate higher density. Along the axes, R varies between 0.2 and 1.5 mm d⁻¹, T varies between 28 and 38 °C, and C_a varies between 350 and 700 ppm. a, c: $T = 28$ °C. b, d: $R = 1$ mm d⁻¹. See Table 1 for the interpretation of the parameters and Appendix A for the value of the parameters not mentioned here.

from a known vegetation pattern in equilibrium with the current climate.

The linear stability analysis in Appendix B is used to identify the analytical range of external forcing and parameter space that produces stable patterns. This analysis does not predict the shape or the extent of the entire patterning area because it focuses on small perturbation growth from a linear analysis. Nonetheless, it provides the minimum range for which stable patterns can form. Using parameter values from Appendix A, the linear stability analysis demonstrates a clear interplay between increased [CO₂], and its concomitant effects – decreased rainfall and increased temperature (Fig. 1a, b). A similar analysis on physiological and soil parameters for current climate (Fig. 1c–e) suggests that the most sensitive parameters for pattern formation are W_0 and k_1 – both linked to the positive feedback mechanism (one for water infiltration, the other for plant water uptake). When taken together, Fig. 1 suggests that for plausible physiological and soil parameter ranges, changes in climatic conditions intersect regions of pattern formation, thereby motivating spatially explicit pattern analysis.

Fig. 2 shows the spatially explicit simulation results for variations in the climatic forcing. The spatial scale of the patterns generated by our model is in the range of a few tens meters, which is in agreement with what is observed in the field (Lejeune et al., 1999; Barbier et al., 2006; Rietkerk et al., 2002). For the specified mean annual rainfall (R) and air temperature (T), increasing [CO₂] leads the system across an area of stable patterns, progressing from bare soil to homogeneous vegetation. The opposite effects are realized with increasing T (but fixing R and [CO₂]) or decreasing R (but fixing T and [CO₂]). Going from homogeneous vegetation to bare soil, a sequence of patterns is crossed: gaps, labyrinths and spots (Fig. 2; Fig. 4 displays each of the pattern shapes in isolation; Okayasu and Aizawa, 2001; von Hardenberg et al., 2001). This sequence is common to all scenarios whether induced by increasing [CO₂] (at constant T and R), increasing R (at constant [CO₂] and T), or decreasing T (at constant [CO₂] and R). This result is in agreement with Gilad et al. (2007a). In their model, the authors showed the equivalence of decreasing the precipitation rate or

biomass growth rate on the one hand to increasing the mortality rate or the evaporation rate on the other hand. A variation in any of these rates has a similar effect on pattern shapes. This also applies to our model, in which growth rate is a function of [CO₂] and mortality is a function of T . Patterns very similar to the labyrinths, gaps and spots obtained in the model have been observed in the field (see aerial pictures of Africa in Rietkerk et al. (2002, 2004) and Barbier et al. (2006)). In the model results, soil moisture patterns are strongly correlated to vegetation patterns (Fig. 2c, d). This is because the positive infiltration feedback is the only positive feedback mechanism between vegetation and soil water availability in our model (see Meron et al. (2007) for the effect of the root-augmentation feedback on the soil water patterns). Comparing with the analytical predictions of Fig. 1, there are clearly patterns ‘outside’ the Turing instability range due to non-linearities of the model. For example, spots (Fig. 2a, b) occur in an area where bare soil is a stable equilibrium, i.e. a bistability area (Fig. 1; von Hardenberg et al. (2001); Rietkerk et al. (2004)). The consequence of these two possible states for the same parameter values (i.e. spots and bare soil) is that going from homogeneous vegetation to bare soil, the system exhibits spot patterns before being transformed to a desert. However, starting from a desert state, the system remains bare (without spots) until transitioning to a labyrinth pattern.

The spatially-explicit model was also run for current climatic conditions but now varying the soil–plant parameters (Fig. 3a–c) to further explore the general shape of the patterns. While we did not conduct this analysis on the entire parameter space, the parameters of Fig. 3 were selected to reflect the key soil (W_0), respiration (R_b), plant hydraulics (k_1), and leaf physiology (g_{CO_2}) attributes. Plants characterized by low R_b (i.e. low respiration), low k_1 (i.e. high resistance to drought) and high g_{CO_2} (i.e. high leaf conductance) are referred to as *high performing* plants, and conversely for *low performing* plants. For high water infiltration rate (high W_0) and low performing plants, vegetation is completely extinct under current climatic conditions (Fig. 3a–c). Lowering W_0 in isolation allows vegetation to survive in a spatially organized way. Indeed, low W_0 initiates runoff in bare areas that can be

